Biomedicine & Pharmacotherapy 142 (2021) 112007

Contents lists available at ScienceDirect

Biomedicine & Pharmacotherapy

journal homepage: www.elsevier.com/locate/biopha

EHP-101 alleviates angiotensin II-induced fibrosis and inflammation in mice

Adela García-Martín [a], Carmen Navarrete [a], Martin Garrido-Rodríguez [b,c,d], María E. Prados [e], Diego Caprioglio [f], Giovanni Appendino [f], Eduardo Muñoz [a,b,c,d,*]

[a] Emerald Health Pharmaceuticals, San Diego, USA
[b] Departamento de Biología Celular, Fisiología e Inmunología, Universidad de Córdoba, Spain
[c] Instituto Maimónides de Investigación Biomédica de Córdoba, Spain
[d] Hospital Universitario Reina Sofía, Córdoba, Spain
[e] Emerald Health Biotechnology España, Córdoba, Spain
[f] Dipartimento di Scienze del Farmaco, Università del Piemonte Orientale, Novara, Italy

ARTICLE INFO

Keywords:
EHP-101
Cannabinoids
Angiotensin II
Cardiac Fibrosis
E2F

ABSTRACT

Some cannabinoids showed anti-inflammatory and antifibrotic activities. EHP-101 is an oral lipidic formulation of the novel non-psychotropic cannabidiol aminoquinone VCE-004.8, which showed antifibrotic activity in murine models of systemic sclerosis induced by bleomycin. We herein examined the effect of EHP-101 on cardiac and other organ fibrosis in a mouse model induced by Angiotensin II. VCE-004.8 inhibited TGFβ- and Ang II-induced myofibroblast differentiation in cardiac fibroblasts detected by α-SMA expression. VCE-004.8 also inhibited Ang II-induced ERK 1 + 2 phosphorylation, NFAT activation and mRNA expression of *IL1β*, *IL6*, *Col1A2* and *CCL2* in cardiac fibroblasts. Mice infused with Ang II resulted in collagen accumulation in left ventricle, aortic, dermal, renal and pulmonary tissues; oral administration of EHP-101, Ajulemic acid and Losartan improved these phenotypes. In myocardial tissue, Ang II induced infiltration of T cells and macrophages together with the accumulation of collagen and Tenascin C; those were all reduced by either EHP-101 or Losartan treatment. Cardiac tissue RNA-Seq analyses revealed a similar transcriptomic signature for both treatments for inflammatory and fibrotic pathways. However, the gene set enrichment analysis comparing data from EHP-101 *vs* Losartan showed specific hallmarks modified only by EHP-101. Specifically, EHP-101 inhibited the expression of genes such as *CDK1*, *TOP2A* and *MKi67* that are regulated to the E2 factor family of transcription factors. This study suggests that the oral administration of EHP-101 prevents and inhibits cardiac inflammation and fibrosis. Furthermore, EHP-101 inhibits renal, pulmonary and dermal fibrosis. EHP-101 could offer new opportunities in the treatment of cardiac fibrosis and other fibrotic diseases.

1. Introduction

Cardiovascular diseases are nowadays the main cause of mortality in the world [1]. Among them, ischemic heart disease and other conditions such as hypertensive heart disease, idiopathic dilated cardiomyopathy and diabetic hypertrophic cardiomyopathy may lead to endomyocardial fibrosis, one of the psychopathological events that causes heart failure [2–4].

Cardiac fibrosis is produced by the accumulation of extracellular matrix (ECM) in the myocardium. The increase of ECM in the myocardium followed by extensive fibrotic remodeling in the ventricle abolishes cardiac contractility and it is associated with the loss of a large number of cardiomyocytes ultimately leading to replacement of dead myocardium with a collagen-based scar [5]. The expression of several

Abbreviations: α-SMC, α-Smooth muscle cell; Ang, Angiotensin; CBD, Cannabidiol; PHDs, Prolyl hydroxylases; CB_1R, Cannabinoid receptor type 1; CB_2R, Cannabinoid receptor type 2; CDK1, Cyclin-dependent kinase 1; Col1a2, Collagen1a2; ECM, Extracellular Matrix; MKi67, Marker of Proliferation Ki-67; RAS, Renin-Angiotensin System; PPARγ, Peroxisome proliferator-activated receptor-γ; SSc, Systemic Sclerosis; TGFβ, Transcription Growth Factor β; TNC, Tenascin C; TOP2A, DNA Topoisomerase II Alpha.

* Corresponding author at: Instituto Maimónides de Investigación Biomédica de Córdoba, Universidad de Córdoba, Avda. Menéndez Pidal s/n. 14004 Córdoba, Spain.

E-mail address: fi1muble@uco.es (E. Muñoz).

https://doi.org/10.1016/j.biopha.2021.112007
Received 12 January 2021; Received in revised form 14 July 2021; Accepted 1 August 2021
Available online 9 August 2021

pro-inflammatory cytokines and pro-fibrotic factors induces differentiation of variety of progenitor lineages including endothelial cells and resident fibroblast to myofibroblast in a process known as endothelial to mesenchymal transition. Myofibroblasts show larger proliferative, contractile, migratory and collagen producing abilities [6]. The activation of inflammation together with the transformation to myofibroblasts produce a high accumulation and synthesis of ECM proteins; the collagen deposition in the myocardium impairs cardiac function and finally leads to heart failure [6].

The renin-angiotensin system (RAS) is the regulatory system of cardiovascular and renal function and its deregulation exerts potent atherosclerotic, inflammatory and fibrotic effects.[7] Angiotensin is the central effector of RAS. It is formed from the enzymatic cleavage of angiotensinogen to Ang I by the aspartyl protease renin. Then, the angiotensin converting enzyme (ACE) converts Ang I to Ang II. [8] Ang II exerts biological activities by binding to the Ang receptor subtypes, Ang receptor 1 (AT1) and Ang receptor 2 (AT2) [8]. Most of the effects of Ang II are mediated by binding to AT1, which is widely present in many tissues and organs, including skin, lung, kidney and heart [9–12]. Moreover, this peptide hormone is a potent proinflammatory agent that modulates immune responses, including T-cell proliferation and differentiation of monocytes into macrophages [13,14]. It is known that Ang II has involved in the evolution of myocardial fibrosis. Indeed, Ang II has been described to be a potent pro-fibrotic molecule [15,16]. In fact, recent studies has seen increased serum levels of Ang II in patients with cardiovascular diseases that are associated with myocardial fibrosis, including hypertension cardiac hypertrophy, atherosclerosis and heart failure [15,17,18].

Following cardiac injury, the immune system plays an important role in repair and regeneration and is implicated in the initiation and regulation of the cardiac fibrotic process including vascular damage [19]. The inflammation is also involved in the transition of cardiac fibroblasts to myofibroblasts, the hallmark of the fibrotic process. A crosstalk between fibroblasts and immune cells is a key step in triggering cardiac fibrosis. Indeed, T cells coordinate and mediate various immune cells activities, including monocytes and macrophages, which are enrolled to the site of the damage contributing to cardiac fibrosis [20]. The excess accumulation of collagen is not only attributed to the myofibroblasts but also macrophages that are directly involved in the deposition of collagen fibers in the myocardium [21]. Overall, the extent of inflammation significantly correlates to the severity of heart failure.

Several lines of evidence have shown that the peroxisome proliferator-activated receptor-γ (PPARγ) and the canonical cannabinoid receptors 1(CB_1R) and 2 (CB_2R) are promising targets for the development of new pharmacological therapies for the treatment of fibrotic diseases.

It has been described that PPARγ ligand agonists reduce oxidative stress and inflammation and as a consequence, may be of therapeutic interest for cardiac fibrosis and to improve vascular endothelial function [22,23]. CB_1R and CB_2R have opposite roles in fibrotic diseases, while activation of CB_1R is profibrotic, the activation of CB_2R is anti-fibrotic in several animal models of fibrotic diseases [24,25].

Previously, we have proven the ability of VCE-004.8, a non-psychotropic aminoquinone derivative synthetic cannabidiol (CBD) acting as a dual agonist of CB_2R and PPARγ, thereby avoiding bleomycin-induced fibrosis [25]. VCE-004.8 inhibited TGFβ-induced Col1A2 gene transcription, collagen synthesis and TGFβ-mediated myofibroblast differentiation [25]. EHP-101 is a lipidic formulation of VCE-004.8 for oral delivery that alleviated bleomycin-induced skin and lung fibrosis. EHP-101 also prevented skin vascular disruption induced by bleomycin and RNAseq analysis showed a clear effect on the inflammatory and epithelial-mesenchymal transition transcriptomic signatures [26,27] completed a Phase I clinical study (clinicaltrial.gov: NCT03745001) and is now under Phase II in SSc patients (ClinicalTrials.gov: NCT04166552). In the present study we show how this formulation prevents Ang-II-induced inflammation and fibrosis in the heart as well as in other organs.

2. Material and methods

2.1. Cell lines and reagents

Immortalized primary human cardiac fibroblasts (hICF) with SV40 Large T antigen were purchased from Innoprot SL (Derio, Spain) and cultured in low passages (< 5 passages). The cells were maintained in a humidified atmosphere at 37 °C containing 5% CO_2, 10% fetal bovine serum (FBS) and 1% (v/v) penicillin/streptomycin in Fibroblast Medium-2 (P60108-2, Innoprot, Derio, Spain). Ang II was purchased from Sigma-Aldrich Co (A9525, Sigma, Madrid, Spain) and TGFβ (Transforming Growth Factor-β)-1 (10 ng/ml) was obtained from ImmunoTools GmbH (Friesoythe, Germany). Ajulemic acid (AjA) was synthesized as described and its purity was >95%. [28] EHP-101 is a lipidic formulation of VCE-004.8 [(1′R,6′R)− 3-(Benzylamine)−6-hydroxy-3′-methyl-4-pentyl-6′-(prop-1-en-2-yl) [1, 1′bi(cyclo-hexane)]− 2′,3,6-triene-2,5-dione)] [26].

2.2. Luciferase assays

hICF cells were transiently transfected for 24 h with the Gal4-Luc reporter plasmid (which includes five Gal4 DNA binding sites fused to the luciferase gene) and the Gal4-$NFAT_{1–415}$ plasmid for 24 h using Roti-Fect (Carl Roth GmbH & Co. KG, Karlsruhe, Germany). Then cells were stimulated for 6 h as indicated. Luciferase activity in the cell lysates was measured as described previously [29] and the specific transactivation expressed as a percentage of activation relative to control.

2.3. Western blots

Cells were preincubated with VCE-004.8, treated with Ang II for 30 min, washed with PBS and proteins extracted in 50 μL of lysis buffer [50 mM Tris-HCl pH 7.5, 150 mM NaCl, 1% (v/v) NP-40, 10% (v/v) glycerol, 10 mM NaF, 1 mM Na_3VO_4, aprotinin (10 μg/ml), leupeptine (10 μg/ml), pepstatin (1 μg/ml) and 1 mM PMSF saturated]. Separated proteins in 10% SDS/PAGE gels were transferred to PVDF membranes and blocked in TBS solution containing 0.1% Tween 20% and 5% bovine serum albumin (BSA) for 1 h at room temperature. Immunodetection of specific proteins was carried out by incubation with primary antibodies against p-ERK (1:1000; # 4695 Cell Signaling Technology), ERK (1:1000, M5670, Sigma) and α-tubulin (1:1000, T9026, Sigma). Membranes were incubated with horseradish peroxidase-conjugated secondary antibody was added and proteins detected by chemi luminescence system (GE Healthcare Europe GmbH).

2.4. Cardiac fibroblasts differentiation

To induce the cardiac fibroblast differentiation into myofibroblast, the cells were plated on glass coverslips with Fibroblast Medium-2 (P60108–2, Innoprot, Derio, Spain). After 24 h in serum depleted media, cells were preincubated with VCE-004.8 for 1 h and stimulated with TGFβ1 (10 ng/ml) or Ang II for another 2 or 48 h. Coverslips were washed with PBS, fixed with methanol: acetone (1:1) and non-specific binding reduced by blocking at room temperature for 1 h with 5% BSA and 0.1% Triton X-100 in PBS. They were then incubated with the primary antibodies overnight at 1:100 dilution. Ki67 antibody was purchased from Abcam (ab15580) and anti-α-Smooth Muscle Actin from Thermo Fischer (#53–9760–80). Coverslips were mounted using Vectashield Antifade Mounting Medium with DAPI (H-1200, Vector Laboratories, Burlingame, Ca, USA) and images obtained using a spectral confocal laser-scanning microscope LSM710 (Zeiss, Jena, Germany) with a 25 × /0.8 Plan-Apochromat oil immersion lens. Images were quantified in 10–15 randomly chosen fields using ImageJ software (rsb.info.nih.gov/ ij/).

2.5. Animals studies

Eight-week-old male C57-BL/6 mice were purchased from Janvier Labs (Cedex, France) and housed with free access to standard food and water under controlled conditions (temperature 20 °C (± 2 °C), 40–50% relative humidity and 12 h light/dark cycle). All experiments were performed in accordance with European Union guideline and approved by the Animal Research Ethic Committee of the Córdoba University (23/03/2018/034). Mice were anesthetized using isoflurane and subcutaneous infusion of Ang II using ALZET® osmotic pump (Model #2004, Charles River, Barcelona, Spain) implanted beneath the midscapular loose skin, delivering Ang II (A9525, Sigma, Madrid, Spain) at 1000 ng kg^{-1} min^{-1} in the case of the preventive model, and at 500 ng kg^{-1} min^{-1} for the therapeutic model. Pumps were left in place for 14 or 28 days in the preventive or therapeutic model, respectively (Supplementary Figure 1A). In the preventive model, starting one day before of the pump implantation, EHP-101 (5, 10 and 20 mg/Kg), Losartan (0.6 g/L) or AjA (5 mg/Kg) were administrated daily by oral gavage. In the therapeutic model, Ang II was infused for four weeks and the treatments, EHP-101 (20 mg/Kg) and Losartan (0.6 g/L) were administered orally daily during the last two weeks of Ang II infusion (Supplementary Figure 1B). Mice were euthanized by cervical dislocation and skin, heart, aorta, lung and kidneys were removed, processed for histological examination or frozen for further analysis.

2.6. Histological and immunohistochemistry analysis

Tissue Section (5 μm-thick) were embedded in paraffin. The left ventricle sections were stained with Sirius red/ Fast green staining (Sigma-Aldrich, Madrid, Spain). First, the sections were incubated in 0.04% Fast Green for 15 min, washed with distilled water, then incubated in 0.1% Fast Green and 0.04% Sirius Red in saturated picric acid for 30 min. For the aorta, kidneys and skin, the sections were stained with picrosirius red (Sigma-Aldrich, Madrid, Spain). Tissues were incubated in 0.1% Sirius Red in saturated picric acid for 60 min for collagen identification. Lung sections were stained with Masson's trichrome (Merck Millipore, Darmstadt, Germany). To analyze the level of fibrosis in lung samples the Ashcroft score was used as previously described [26,27,30]. The sections were then dehydrated and mounted with Eukitt Mounting Medium (Sigma-Aldrich, Madrid, Spain). Three to four random fields of each tissue section were photographed using a Leica DFC420c camera by standard brightfield microscopy and evaluated using Fiji software (rsb.info.nih.gov/ij/). For immunohistochemistry, heart sections (left ventricle; 5 μm-thick) were deparaffinized and boiled in sodium citrate buffer for 10 min (10 mM, pH 6.0) for antigen retrieval. Next, incubated three times for 10 min in a Phosphate Buffer Saline (PBS) washing buffer containing 0.1% Tween and incubated overnight at 4 °C with the following antibodies: for immunohistochemical detection of TNC (an extracellular matrix protein involved in fibrosis development), anti-TNC antibodies (1:100, #MAB2138, RD system, Minneapolis, MN, USA), for T-lymphocyte and macrophage infiltration, anti-CD3 antibodies (1:50, SC-20047, Santa Cruz Biotechnology) or anti-F4/80 antibodies (1:50, #MCA497, Bio Rad Laboratories, Hercules, CA, USA), respectively. The slides were incubated with the appropriate biotin-conjugated secondary antibody for 1 h at room temperature: goat anti-rat (BP-9400, Vector Laboratories, Burlingame, CA, USA) for anti-TNC anti-F4/80 and goat anti-mouse (21538, Merck-Millipore) for anti-CD3. Negative controls were incubated only with PBS. Reaction products were detected by avidin-biotin-peroxidase (Vector Laboratories), the color reaction was developed with DAB (3,3′ diaminobenzidine) chromogen (Dako, Santa Clara, CA, USA), subsequent counterstaining with haematoxylin (Sigma-Aldrich) and mounting with Eukitt Mounting Medium (Sigma-Aldrich). Three to four random fields were digitized using a Leica DFC420c camera and analyzed using Image J software by two independent observers.

2.7. Confocal analysis

Sections of heart tissue (5 μm) were deparaffinized with sodium citrate buffer, washed three times during 10 min in PBS buffer containing 0.1% Triton X-100 and blocked with 3% BSA. They were then incubated with the primary antibodies overnight at 1:100 dilution. Ki67 antibody was purchased from Abcam (ab15580) and anti-α-Smooth Muscle Actin from Thermo Fischer (#53–9760–80). The next day sections were washed three times during 10 min with a wash buffer and incubated (1:100 dilution) in darkness at room temperature during 1 h with secondary antibody anti-rabbit Texas Red from Thermo Fischer (#A-6399). Finally, sections were mounted using Vectashield Antifade Mounting Medium with DAPI and images obtained using a spectral confocal laser-scanning microscope LSM710 (Zeiss) with a 63 × Plan-Apochromat or 25 × /0.8 Plan-Apochromat oil immersion lens.

2.8. RT-qPCR

The total RNA from frozen mouse heart tissue was isolated and purified using QIAzol lysis reagent (Qiagen, Hilden, Germany) and RNeasy mini kit (Qiagen). Cardiac Fibroblasts (5 $\times 10^4$ cells/cm^2) were pre-incubated with VCE 004.8, stimulated with Ang II for either 2 or 24 h and total RNA was extracted using High Pure Isolation Kit (Roche Diagnostic, Switzerland). Total RNA (1 μg) was retrotranscribed using the iScriptTM cDNA Synthesis Kit (Bio-Rad) and the cDNA analyzed using a CFX96 Real-Time PCR Detection System (Bio-Rad) by real-time PCR using the iQTM SYBR Green Supermix (Bio-Rad). Human *HPRT* was used for *in vitro* studies and mouse *Gadph* or *Eef2* housekeeping genes were used to standardize the mRNA expression levels in each sample. Expression levels were calculated using the 2-ΔΔCt method. Sequences of oligonucleotide primers are shown in Table 1.

2.9. RNA-Seq analyses

RNA samples isolation was performed from myocardial tissue as described above and 300 ng of RNA per sample were used to construct a cDNA library capturing mRNA through Oligo-dT beads with polyA tails (Illumina TruSeq RNA Library Prep Kit v2, #RS-122–2001). The cDNA library was sequenced on an Illumina Hiseq 2500 system, generating single end 50 bp reads and obtaining ~30 million reads per sample.

2.10. RNA-Seq bioinformatic analysis

Raw reads were pre-processed with fastp (v0.20.0) [31] using a trimming window size of 4 bp with a required mean quality of 15 and a required total length of 20 bp for a read to pass the filter. Then, reads were aligned against the GRCm38 genome (v84) from ENSEMBL with HISAT2 (v2.1.0) [32]. The count matrix was obtained from the alignments using the corresponding ENSEMBL annotation file with featureCounts (v2.0.0) [33]. Normalization and differential expression analyses were performed with edgeR (v3.30.0) [34] excluding genes with less than 15 counts across all samples. Functional analysis was then performed through a gene set enrichment analysis with the fgsea package (v1.14.0), ranking genes by the edgeR estimated log transformed fold change and using the functional categories defined by MSigDb hallmarks for Mus musculus (V7.0) [35].

2.11. Accession numbers

Raw reads and the count matrix are available at the Gene Expression Omnibus (GEO) web site (https://www.ncbi.nlm.nih.gov/geo) using accession number GSE151466.

2.12. Statistical analysis

Statistical analyses were performed using GraphPad Prism version

Table 1
Sequences of mouse (m) and human (h) RT-PCR primers.

Gene	Forward	Reverse
mIl-6	5´-GAACAACGATGATGCACTTGC-3´	5´-TCCAGGTAGCTATGGTACTCC-3
mI-1β	5´-CTCCACCTCAATGGACAGAA-3´	5´-GCCGTCTTTCATTACACAGG-3´
mTnc	5´-ATCCCTTCATCAGCAGTCCA-3´	5´-GCATCCGTACCAAAACCATC-3´
mCdk1	5´-CAGAGATTGACCAGCTCTT-3´	5´-GAAAGGTGTTCTTGTAGTCC-3´
mTop2a	5′-CGGAATGACAAGCGAGAAGTAA-3′	5′-GCATTGTAAAGATGTATCGTGGAC-3′
mMki67	5´-AATCCAACTCAAGTAAACGGGG-3´	5´-TTGGCTTGCTTCCATCCTCA-3´
mGapdh	5´-TGGCAAAGTGGAGATTGTTGCC-3´	5´-AAGATGGTGATGGGCTTCCCG-3´
mEef2	5´-TGTCAGTCATCGCCCATGTG-3´	5´-CATCCTTGCGAGTGTCAGTGA-3´
hIL1β	5´-GACCTTCCAGGATGAGGACA-3´	5´-AGCTCATATGGGTCCGACAG-3´
hIL6	5´-GGTACATCCTCGACGTGTCT-3´	5´-GTGCCTCTTTGCTGCTTTCAC-3´
hCOL1A2A	5´-CCGTGCTTCTCAGAAGACAG-3´	5´-CTTGCCCCATTCATTCATCA-3´
hCCL2	5´- CCCCAGTCACCTGCTGTTAT-3´	5´-TGG AAT CCT GAA CCC ACT TC-3´
hHPRT	5´-ATGGGAGGCCATCACATTGT-3´	5´-ATGTAATCCAGCAGGTCAGCAA-3´

8.00 (GraphPad, San Diego, CA, U.S.A.). Data from the *in vivo* experiments are expressed as median ± interquartile as the mean, tested for normal distribution using Shapiro-Wilk normality test and analyzed using one-way ANOVA followed by Bonferroni's *post hoc* test. Kruskall-Wallis followed by Dunn's post-hoc test was used to calculate significant differences with data not normally distributed. $P < 0.05$ was set as minimal statistical significance.

3. Results

3.1. Effect of VCE-004.8 and Losartan on angiotensin II-induced cardiac myofibroblast differentiation and signalling

The profibrotic activity of Ang II on cardiac fibroblasts *in vitro* and *in vivo* has been extensively documented [6,12]. To study myofibroblast differentiation *in vitro*, immortalized cardiac fibroblasts (hICF) were stained with for α-SMA expression, a specific marker for myofibroblasts differentiation. As shown in Fig. 1A, both TGF-β and Ang II induced α-SMA protein expression in cultured hICF and pretreatment with VCE-004.8 (5 μM) decreased α-SMA expression. The differentiation to myofibroblast was associated with morphological changes of cellular hypertrophy. We observed cell shape variations from spindle-shaped and they exhibited a dendritic morphology compared to cells treated with Ang II or TGFβ, which were more spread, hallmark of myofibroblast differentiation. To further study the effect of VCE-004.8 on Ang II signaling pathways in hICF, we analyzed ERK1 + 2 and NFAT activation, two pathways activated by Ang-II [36]. VCE-004.8, as well as Losartan, inhibited both Ang II-induced ERK1 + 2 phosphorylation and NF-AT activation in hICF (Fig. 1B and C). We also found that VCE-004.8 inhibited the mRNA expression of *IL1β*, *IL6*, *Col1A2* and *CCL2*, induced by Ang II or TGFβ in hICF cells (Fig. 1D).

3.2. EHP 101 and Ajulemic acid prevented interstitial and perivascular myocardial collagen deposition induced by Ang-II infusion

In C57-BL/6 mice, Ang-II infusion for two weeks significantly increased collagen deposition in the left ventricle, particularly in the interstitial and perivascular areas. Treatment with EHP-101 initiated at the same time as Ang II infusion (preventive model) attenuated interstitial cardiac fibrosis as well as perivascular fibrosis in a dose-dependent manner and similar results were observed in the heart of mice administered with Losartan (0.6 gr/L). AjA, another synthetic cannabinoid targeting CB_2R and PPARγ [28,37] also prevented interstitial and perivascular fibrosis although with lower efficacy compared to EHP-101. To analyze total collagen, Picrosirius red staining was used (Fig. 2A and B).

3.3. EHP-101 ameliorated Ang II-induced aortic, kidney and skin fibrosis in a preventive model of fibrosis

It has been described that Ang II induces fibrosis on internal organs and skin [9–12]. Thus, we performed histochemical studies in order to investigate the effects of EHP-101 in the preventive model of Ang II-induced organ fibrosis. In aortic vessel, the collagen content in the adventitial layer was increased in mice infused with Ang II (0.6 units *vs* 0.375 units in control group) and the media layer thickness was significantly reduced by both EHP-101 treatment (0.425 units) or Losartan (0.38 units) (Fig. 3A). The area between the external elastic lamina and the tunica externa is called the adventitia area, which is the outermost layer of the vessel. We examined also the effect of the treatments on renal fibrosis by Masson's trichrome and picrosirius red staining. Kidneys of mice infused with PBS showed low levels of collagen deposition (6.94% collagen area and 2.69% fibrotic area) (Fig. 3B). However, collagen accumulation and augmentation of fibrotic area in the interstitial sites was clearly detected in kidneys of mice subjected to Ang-II infusion (29.11% collagen area and 18.22% fibrotic area). Collagen deposition and fibrotic area were significantly reduced by treatment with either EHP-101 (3.78% collagen area and 6.43% fibrotic area) or Losartan (0.6 g/L) (11.97% and 8.08% collagen and fibrotic area respectively) (Fig. 3B).

We have previously shown that EHP-101 alleviates dermal fibrosis through PPARγ and CB_2R receptor-dependent pathways in a mice model of SSc [26,27]. Thus, we investigated the effect of oral EHP-101 in dermal fibrosis induced by Ang II. Picrosirius red staining indicated that collagen fibers were more closely packed in Ang II infused mice (37.95%) compared with control saline infused mice (20.69%), reflecting increased collagen and extracellular matrix deposition (Fig. 3C). The deposition of collagen fibers was attenuated with either EHP-101 (28.17%) (20 mg/Kg) or Losartan (0.6 g/L) (19.03%) treatments.

3.4. Pharmaco-transcriptomic signature of EHP-101 and Losartan in cardiac tissue

In order to obtain a global perspective of the effect of EHP-101 on cardiac fibrosis, we performed a detailed study of the tissue transcriptome changes in response to Ang II, Ang II +EHP-101 and Ang II + Losartan. Thus, we used a mRNA-Seq approach to obtain a total of 16,163 genes with more than 15 counts across all samples, which were considered for further analyses. Following the differential expression analysis with edgeR, the functional analysis revealed complementary signature for transcriptomic hallmarks related with the inflammatory and fibrotic processes, which were up-regulated in response to Ang II and down-regulated with both treatments (EHP-101 and Losartan). Some examples can be found in the Figs. 4A and 5A, as "Inflammatory response" and "Epithelial mesenchymal transition" (fgsea adjusted P value < 0.05). Then, to study those changes at the gene level, we used the leading-edge analysis to determine which features were driving the

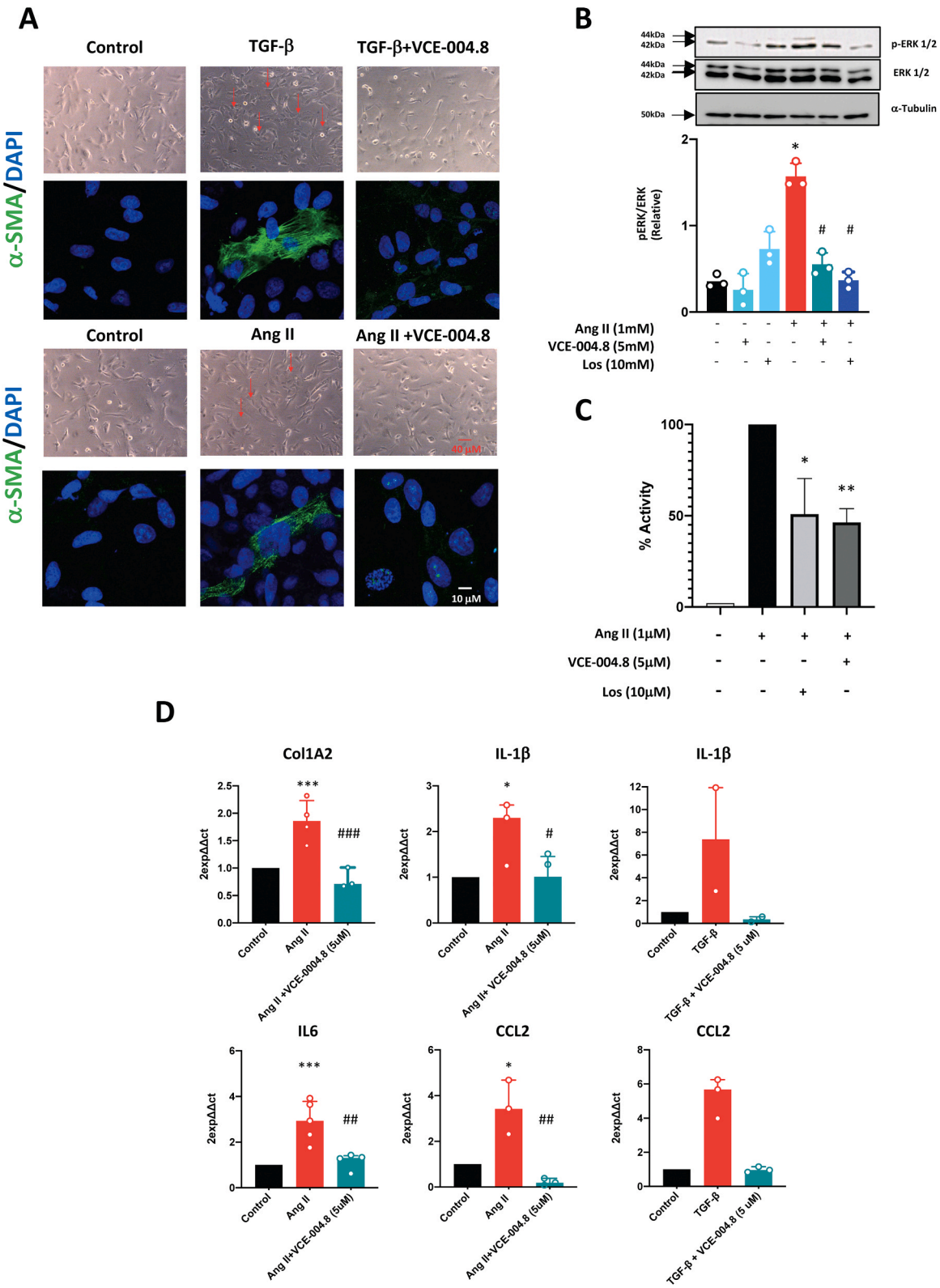

Fig. 1. VCE-004.8 prevents cardiac fibroblasts differentiation into myofibroblasts. A. Representative images of cardiac fibroblasts differentiation into myofibroblasts induced with Ang II or TGFβ and treated with VCE-004.8. B. Western blot images showing inhibition of p-ERK after treatment with VCE-004.8 or Losartan. C. Effect of VCE-004.8 on NF-AT transcriptional activity. hICH cells were transfected with a GAL4-NFAT expression plasmid plus a GAL4-Luc reporter plasmid. Cells were preincubated with the VCE-004.8 or Losartan for 20 min and stimulated with Ang II (1 μM) for 6 h. Cells were lysed for luciferase activity. Results are presented as the percentage of luciferase activity relative to control (100% for Ang II treatment). D. The mRNA expression of genes (*IL1β*, *IL6*, *COL1A2* and *CCL2*) was quantified by qPCR and normalized to the levels of HPRT. Cells were incubated with VCE-004.8 for 1 h following Ang II or TGF-β for 2 or 24 h. Data represent the mean ± SEM, and significance was determined by Kruskall-Wallis followed by Dunn's post-hoc test. ***$p < 0.001$, **$p < 0.01$ and *$p < 0.05$ *vs* control; *###p< 0.001*, ##$p < 0.01$ and $p < 0.05$*vs* Ang II.

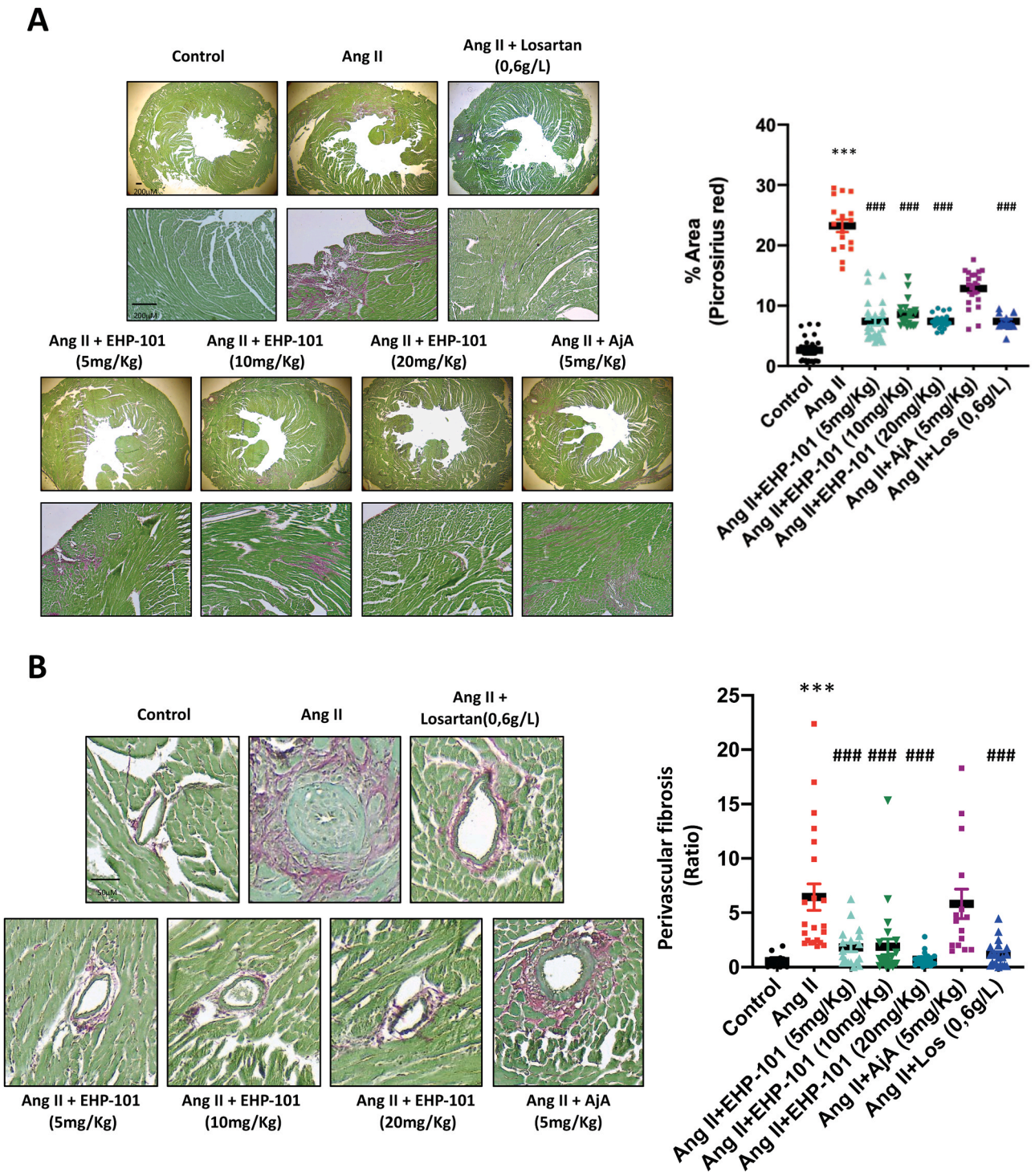

Fig. 2. EHP-101 prevents cardiac fibrosis. A. Representative images of picrosirius red/green fast stained left ventricle sections of the preventive model, interstitial and perivascular area showing collagen accumulation in purple (upper and middle and bottom panel respectively). B. Quantification of collagen accumulation interstitial and perivascular in heart. In order to normalize for vessel size, a ratio of adventitial area/vessel area was calculated and represent the normalized perivascular fibrotic area. Values are expressed as median ± interquartile range with statistical comparison. For all these area measurements, three to four sections from 3 to 7 mice per group were analyzed. Ang II–treated wild-type mice and all other conditions. ***$p < 0.001$ *vs* control group; ###$p < 0.001$, *vs* Ang II group.

observed results. Hence, we obtained three lists of genes for the "Inflammatory response" and "Epithelial mesenchymal transition" hallmarks, one per contrast, which showed an overlap of 52 and 64 genes, respectively (Fig. 5B). The expression values for the first 25 leading edge genes in response to Ang II are shown on the Fig. 4B. In order to confirm these results, the expression of selected genes connected to inflammation and fibrosis was studied by RT-qPCR. As expected, Ang II-infused mice showed significantly higher expression levels of *Tnc*, *Il6* and *Il1β* in cardiac left ventricle compared to the control group. Mice treated with either EHP-101 or Losartan showed a significantly reduced up-regulation (Fig. 4C).

To confirm the inhibitory effects of EHP-101 on inflammation and fibrosis, we analysed the infiltration of T cells ($CD3^+$ cells) and macrophages ($F4/80^+$ cells) in the heart left ventricle. As depicted in Fig. 4D,

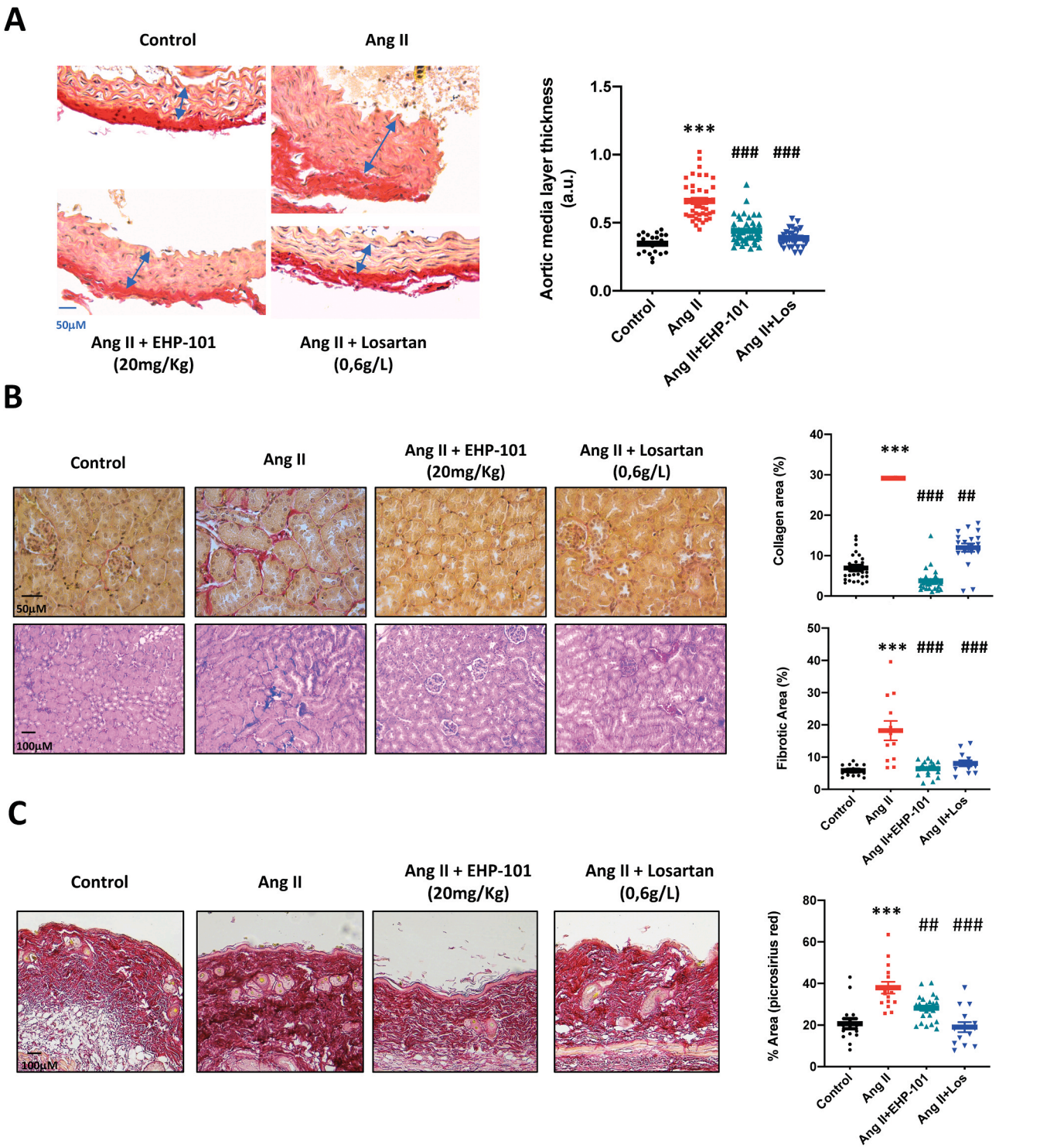

Fig. 3. EHP-101 treatment prevents increase aortic media thickness, renal and skin fibrosis induced by Ang II. A. Representative images of aortic sections for Sirius red in preventive model (left panel) and the quantification of respective measurements on aorta sections (right panel). Blue arrows indicate aortic media B. Representative photomicrographs of renal tissue from Ang II mouse preventive model stained with picrosirius (upper left panel) red and Massoń's trichome (bottom left panel) and representative results for quantification of respective measurements of collagen area and fibrotic area respectively in kidney (right panel). C. Representative photomicrographs of dermal tissue stained with picrosirius red (left panel) and results for quantification of respective measurements of collagen area in skin. Data are expressed as median ± interquartile range with statistical comparison between Ang II–treated wild-type mice and all other conditions. For all these area measurements, three to four sections from three to five mice per group were analyzed. ***$p < 0.001$ *vs* control group; ###$p < 0.001$, ##$p < 0.01$ *vs* Ang II group.

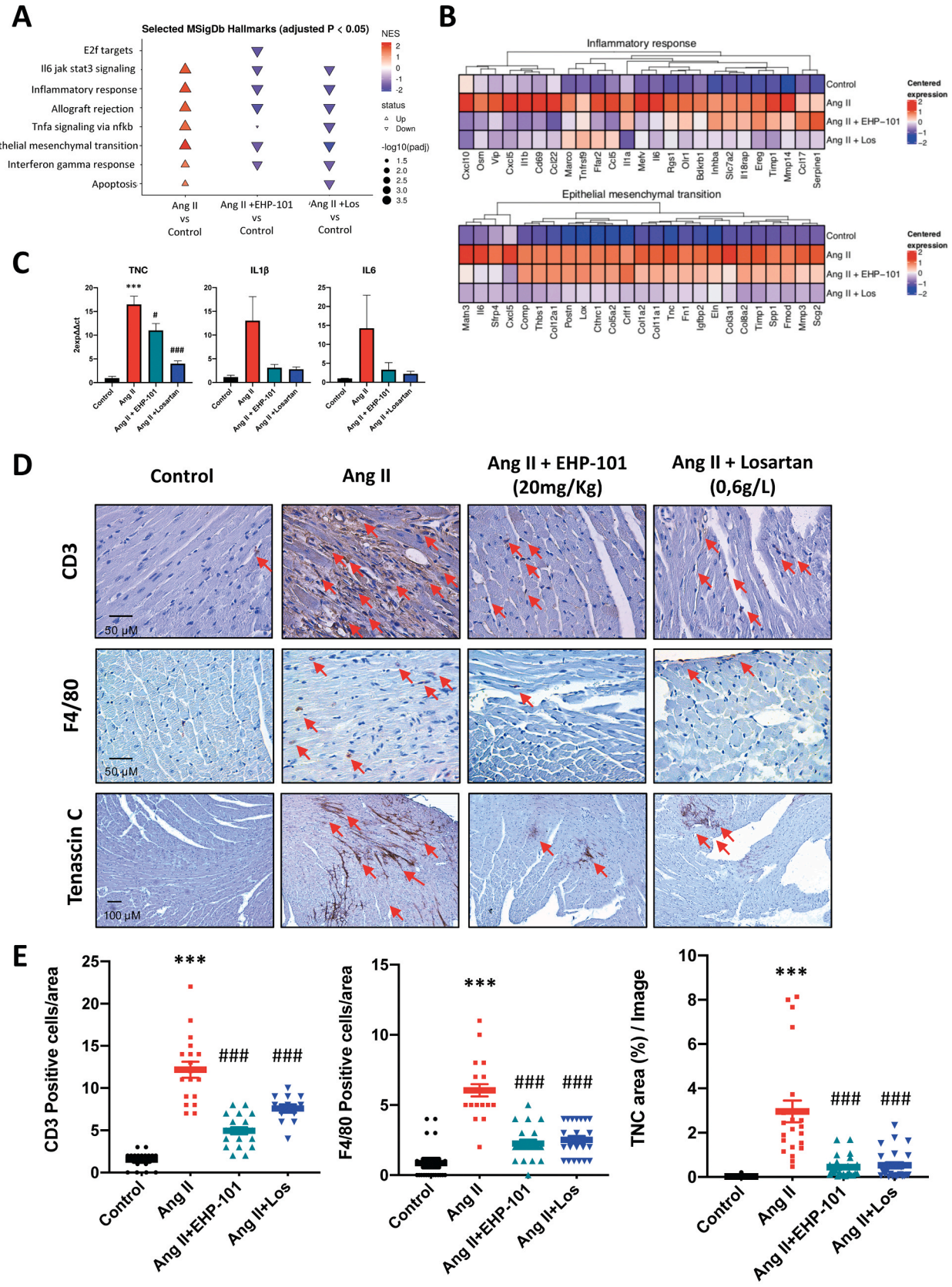

(caption on next page)

Fig. 4. EHP-101 alleviated inflammation and fibrotic markers in heart. A. Gene set enrichment analysis results. The dot plot shows the selected significantly altered hallmarks (Y axis) per contrasts (X axis). The arrow shape, size and color indicate the direction, significance and normalized enrichment score for each result, respectively. Only results with an adjusted *P* value <0.05 are shown. B. Gene expression values for the top 25 leading edge genes within the hallmarks "Inflammatory response" and "Epithelial mesenchymal transition" at the Ang II *vs* Control contrast. The heatmap color indicates the mean of the scaled expression values after normalization. C. Gene expression of profibrotic and pro-inflammatory genes including *Il6*, *Il1β*, and *Tnc* were measured by RT-qPCR. Expression levels were calculated using the 2-ΔΔCt method. Values are expressed as mea ± SEM for three animals per group. ***$p < 0.001$ *vs* control group ###$p < 0.001$, #$p < 0.05$*vs* Ang II group. D. Representative images of CD3 + T-lymphocyte infiltration, F4/ 80 + macrophages and Tenascin C (TNC) in the heart detected by immunostaining. E. Representative results quantified and expressed as CD3 (+) cells/area, F4/80(+) cells/area and TNC percentage of area/image. Results are expressed as median ± interquartile range with statistical comparison between Ang II–treated wild-type mice and all other conditions. For all these area measurements, three to four sections five to seven mice per group were analyzed. ***$p < 0.001$ *vs* control group; ###$p < 0.001$ *vs* Ang II group.

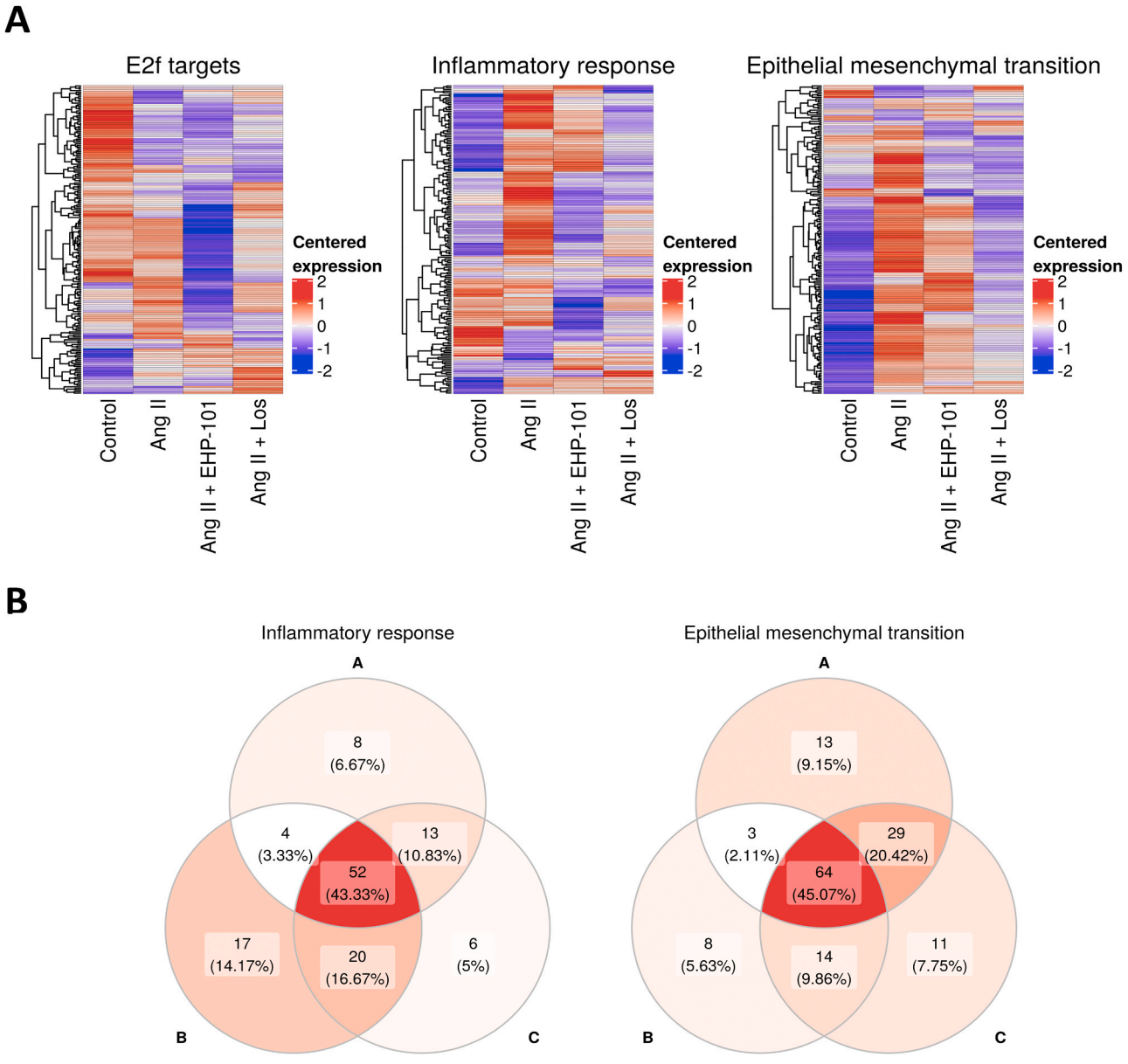

Fig. 5. Gene expression values for all the genes included in the "Inflammatory response", "Epithelial mesenchymal transition" and "E2F targets" hallmarks. The heatmap color indicates the scaled expression values after normalization. B. Overlap between the leading-edge genes for each contrast on the "Inflammatory response" and "Epithelial mesenchymal transition" hallmarks, being A) Ang II *vs* Control, B) Ang II + EHP-101 *vs* Ang II and C) Ang II + Los *vs* Ang II.

we found an increase of infiltrated T cells and macrophages in Ang-II infused group in comparison with control saline infused mice. The number of T cells and macrophages was reduced by the oral treatment with both EHP-101 and Losartan. Moreover, immunohistochemistry confirmed that cardiac expression of TNC was absent in the heart of animals infused with saline and significantly increased in Ang II challenged mice. However, oral administration of EHP-101 reduced Ang II–induced TNC protein expression to levels similar to those of Losartan (Fig. 4D and E).

In addition to this complementary signature for hallmarks related with inflammation and fibrosis, the mRNA-Seq analysis also revealed a group of transcriptomic alterations which occurred only in response to

EHP-101 treatment. The top 10 altered hallmarks for the Ang II + EHP-101 *vs* Ang II contrast are shown in the Fig. 6A. The down-regulation of the "E2F targets" with EHP-101 is important, given the regulatory role of this family of transcription factors in the cardiac fibrotic process [38]. As previously done with the other hallmarks, the leading-edge analysis was used to determine which genes were responsible for this result. In Fig. 6B, we show the expression values for the first 25 leading edge genes on this functional category for the Ang II + EHP-101 *vs* Ang II. To further confirm this result, we evaluated the expression level of genes related to E2F targets hallmark such as Cyclin-dependent kinase 1 (*Cdk1*), DNA Topoisomerase II Alpha (*Top2a*) and Marker of Proliferation Ki67 (*Mki67*). Quantitative real-time polymerase chain reaction revealed a reduction on gene expression levels in the EHP-101 administered group as compared with Ang II infused mice (Fig. 6C). Ki67 expression was also induced by Ang II in hICF and prevented by the pretreatment with VCE-004.8 (Fig. 6D). Moreover, and consistent with the antifibrotic effect of EHP-101, there was a significant reduction of expression of α-SMA in EHP-101-treated mice in comparison with Ang-II-infused mice (Fig. 6E). In addition, *Mki67* expression changes were confirmed at the protein level by immunofluorescent staining for *Mki67*. The number of $Ki67^+$ cells were increased in Ang-II infused mice and significantly reduced by EHP-101 but not by Losartan (Fig. 6F).

3.5. EHP-101 alleviated Ang II-induced perivascular cardiac, aortic, kidney and lung fibrosis and cardiac immune cells infiltration in the therapeutic model of fibrosis

Next, we evaluated the potential therapeutic effect of EHP-101 on fibrosis. Mice were infused with Ang II (500 ng Kg^{-1} min^{-1}) for four weeks and EHP-101 treatment was administered daily only for the last two weeks. As shown in Fig. 7A, the collagen accumulation on interstitial and perivascular myocardial determined by picrosirius red staining was augmented in mice infused with Ang II (32.77% area and perivascular ratio of 3.3) in comparison to control mice infused with saline (16.8% area and perivascular ratio of 0.34). Collagen deposition was significantly attenuated in mice treated with either EHP-101 (20 mg/Kg) (13.53% area and perivascular ratio of 1.28) or Losartan (0.6 g/L) (16.2% area and perivascular ratio of 1.26) compared with the Ang II group. Next, we analyzed the infiltrated T cells ($CD3^+$) and macrophages ($F4/80^+$) in the left ventricle. Ang II induced a significant increase in the number of $CD3^+$ T-lymphocyte infiltration into the heart compared to control mice (Fig. 7B), which was significantly reduced by either EHP-101 or Losartan treatment. Similarly, macrophage infiltration into the left ventricle was extensively observed in both interstitial and perivascular regions in Ang II–infused mice and reduced by both treatments (Fig. 7C).

Furthermore, Ang II infusion for four weeks increased aortic medial thickness mediated by collagen deposition (approximately 2-fold) in comparison with control mice (Fig. 8A), which was attenuated by oral EHP-101 (1.3-fold) and by Losartan (1.26-fold) treatments. The antifibrotic effect of EHP-101 was also evaluated in the kidneys. Kidneys of mice infused with Ang II for 4 weeks showed an increase in collagen accumulation (27.37%) compared to mice infused with saline (15.3%). Kidney fibrosis in Ang II-challenged mice was greatly reduced by the treatment with EHP-101 (21.06%) but not by Losartan (24.16%) (Fig. 8B).

There is significant evidence that Ang II induces pulmonary fibrosis in animal models [10]. Therefore, we explored the therapeutic potential of EHP-101 on lung fibrosis. We confirmed that Ang II-infused mice developed lung fibrosis in the pulmonary parenchyma, as assessed histologically by Massonś trichrome staining and determined by Ashcroft score (from 4.6 to 2.6 score). Both EHP-101 and Losartan significantly alleviated lung fibrosis (Fig. 8C). Collectively, our results demonstrate that administration of EHP-101 in the therapeutic model reduced Ang II–induced fibrosis in several internal organs.

4. Discussion

In previous publications, we have shown the development of the compound of VCE-004.8, which is a dual agonist for PPARγ/CB_2R able to inhibit HIF prolyl hydroxylases (PHDs) [25,39]. This is an example of how synthetic derivatives from cannabinoids with improved bioactivities can be used in the field [40]. In this sense, in this work we have studied the effect of EHP-101 on preventive and therapeutic models of organ fibrosis induced by Ang II. Specifically, EHP-101 was able to alleviate cardiac, aortic, lung, kidney and skin fibrosis that paralleled a significant reduction in the infiltration of inflammatory cells in the heart of Ang II-challenged mice.

In many fibrotic diseases, tissue inflammation precedes fibrosis and, therefore, it is possible that the anti-inflammatory activity of EHP-101, mediated through CB_2R and PPARγ, may inhibit T-cell and macrophage activation [26,27]. Ang II is a potent vasoconstrictor that increases AT1 receptor expression and promotes fibrosis in the skin and internal organs [9–12]. Moreover, this peptide directly activates cells and inflammatory signals that trigger the fibrogenesis machinery, promoting proliferation of myofibroblasts and accumulation of ECM, such as collagen. [7,12,41]. Here, we found that EHP-101 alleviated fibrosis in the internal organs of Ang II induced mouse fibrosis models, and that VCE-004.8 may prevent AT1 and/or AT2 signalling in cardiac fibroblasts. This mitigation of the fibrogenesis could be promoted by the PPARγ ligand action of EHP-101. In fact, PPARγ ligands ameliorate fibrogenesis and collagen accumulation, inhibiting skin and organ fibrosis, including cardiac fibrosis [23,25–27,42]. We and others have also shown that CB_2R agonists exert antifibrotic effects on multiple internal organs and the skin [25–27,43]. On the other hand, HIF-1α activation, which can be induced by PHDs inhibition, has been observed to support wound healing through regulation of inflammation, angiogenesis and vasculogenesis in acute injury [44]. Moreover, the HIF-dependent gene, erythropoietin (EPO) gene, provides efficient protection against renal fibrosis [45]. The ability of VCE-004.8 to inhibit PHDs may also account for its antifibrotic activity since it has been shown that conditional ablation of PHD2 in myeloid lineage attenuates hypertensive cardiovascular hypertrophy and fibrosis [46].

In the same sense, in a model of ventricular dysfunction, the treatment with a selective HIF PHD inhibitor (GSK360A) after myocardial infarction improves ventricular function [47]. Other studies in mice have shown that HIF-1α activation and increased levels of the Vascular endothelial growth factor in cardiac tissue reduce cardiac hypertrophy and myocardial fibrosis induced by pressure-overload [48]. Interestingly, the efficacy of EHP-101 seemed to be superior to AjA, another cannabinoid with dual PPARγ/CB_2R agonistic activity, which is the active ingredient of Lenabasum®, a drug candidate for the treatment of diffuse cutaneous Systemic Sclerosis [49]. Since AjA does not signal through the HIF pathway, our results further support the possibility that this pathway is importantly involved in the therapeutic effect of EHP-101 as suggested previously in a murine model of SS induced by bleomycin [27]. Nevertheless, the exact mechanism of action for EHP-101 (VCE-004.8) in Ang-II-induced organ fibrosis requires further research using genetic or pharmacological models.

Previous evidence indicates that inflammation is an early event and plays a fundamental role in development of cardiac fibrosis [1]. Ang II induces infiltration of inflammatory cells in the myocardium, thus initiating remodeling and consequently cardiac fibrosis [21,50]. The components of inflammation include macrophages and T cells that are associated with secretion of cytokines, such as IL1β, IL6 and TGF-β. They also include extracellular matrix protein deposition, such as Collagen and TNC that are the hallmark for cardiac fibrosis development [50–52]. Herein, our results demonstrate that EHP-101 reduces the infiltration of inflammatory cells and fibrosis in the left ventricle, in both preventive and therapeutic models of Ang-II-induced fibrosis in mice.

Interestingly, we observed a specific downregulation by EHP-101 of a group of genes that are classified as the "E2F targets" hallmark. The

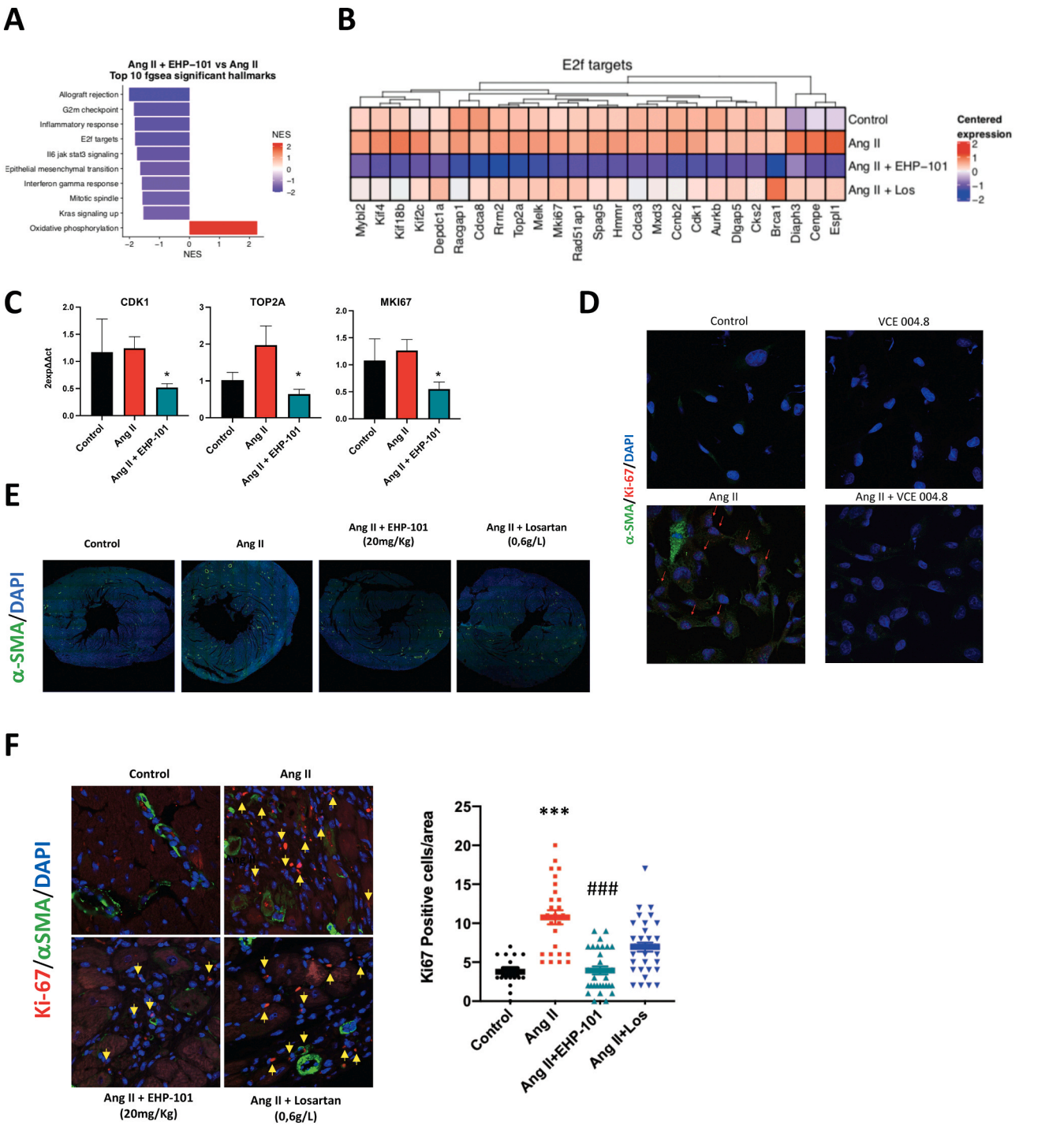

Fig. 6. Inhibitory effect of EHP-101 on E2F pathway and cardiac myofibroblast. A. Top 10 significant hallmarks at the Ang II + EHP-101 *vs* Ang II contrast. The hallmarks (Y axis) are ordered by their normalized enrichment score (X axis). Only results with an adjusted P value < 0.05 are shown. B. Gene expression values for the top 25 leading edge genes on the hallmark "E2F targets" at the Ang II + EHP-101 *vs* Ang contrast. The heatmap color indicates the mean of the scaled expression values after normalization. C. Gene expression on the E2F pathways markers including *Cdk1*, topoisomerase 2-alpha (*Top2a*) and *Mki67* were measured by RT-qPCR. Expression levels were calculated using the 2-ΔΔCt method. Values are expressed as mean- ± SEM for at least seven animals per group. $*p < 0.05$ *vs* Ang II group. D. Representative images of hICF differentiation into myofibroblasts. Cells were pretreated with VCE-004.8 for 1 h and stimulated with Ang II (1 μM) for 2 h. hICF were stained for α-SMA (green), Ki67 (red) and DAPI (blue). E. Immunofluorescence labelling of smooth muscle cells (α-SMA, green fluorescence) in heart. F. Representative immunofluorescence images of myofibroblast proliferation in left ventricular section stained with Ki67 (red fluorescence). Cells are marked by yellow arrows (left panel). Quantification of number of Ki67-positive cells from 5 to 10 fields per heart (right panel). Four animals from each group were analyzed. Data are presented as median ± interquartile range with statistical comparison between Ang II–treated wild-type mice and all other conditions. $***p < 0.001$ *vs* control group; $###p < 0.001$ *vs* Ang II group.

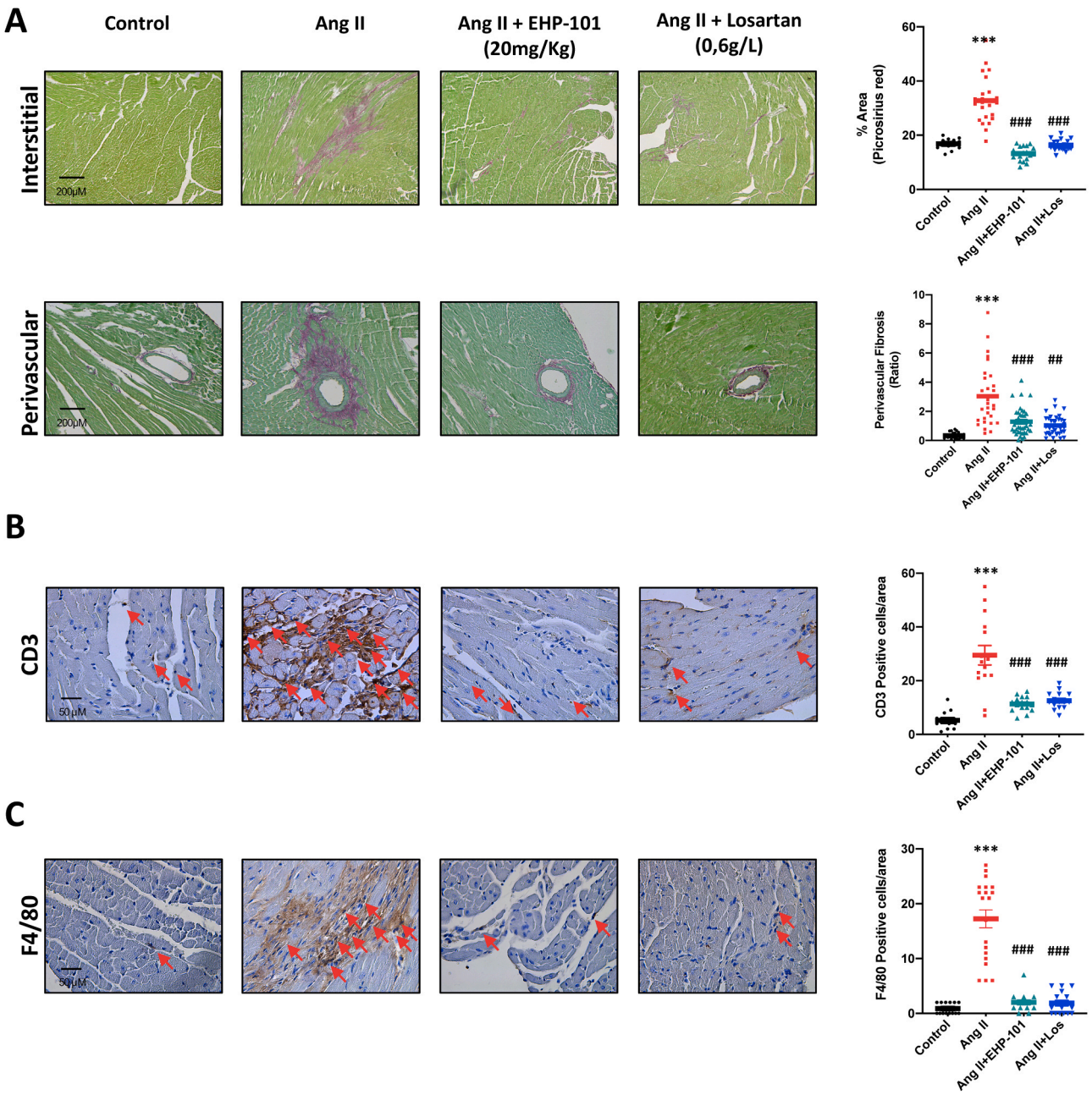

Fig. 7. Therapeutic EHP-101 effect on cardiac fibrosis. A. Representative images of picrosirius red/green fast stained left ventricle sections, interstitial and perivascular area showing collagen accumulation in purple (left panel) and their quantification of collagen accumulation interstitial and perivascular in heart (right panel). The ratio of adventitial area/vessel area was calculated and represent the normalized perivascular fibrotic area Values are expressed as median ± interquartile range with statistical comparison. B. Representative images of CD3 + T-lymphocyte infiltration in cardiac tissue detected by immunostaining and quantified results expressed as CD3 (+) cells/area (right panel). C. Representative images of F4/80 + macrophages in the heart detected by immunostaining and quantified results expressed as F4/80(+) cells/area (right panel). For all these area measurements, three to four sections from a sample from four to eight mice per group were analyzed ***$p < 0.001$ *vs* control group; ###$p < 0.001$, ##$p < 0.01$ *vs* Ang II group.

E2F family of transcription factors plays a crucial role in controlling the expression of genes involved in cell proliferation, differentiation, and apoptosis [53]. A recent study indicated that the modulation of *CDK1*, a known target of the E2F pathway, is involved in G1 checkpoint regulation, which inhibits the proliferation of cardiac fibroblast, thus exerting a protective effect on cardiac fibrosis [54]. Moreover, the expression and activity of E2F molecules have been detected in the development of myocyte hypertrophy and blocking E2F function inhibits the death of cardiomyocytes [55]. It is likely that EHP-101 through the E2F pathway could ameliorate the proliferation of myofibroblasts and the hypertrophy of cardiomyocytes induced by Ang II infusion.

The Ang II signal transduction process is known to produce both inflammation and fibrosis, by promoting the endoplasmic reticulum stress and activating the nuclear factor-κB and TGF-β-related signaling pathways [8]. Our transcriptomic analysis has shown that both the EHP-101 and Losartan treatments were able to normalize the expression of some genes such as *Il1β*, *Il1α* or *Il6*, reflecting the activity of infiltrated T cells and macrophages in the cardiac tissue [50]. On the other hand, the diminished expression levels of genes such as *Tnc* [51], Collagen *(Col)1a2* and Fibronectin1 (*Fn1*) would be the consequence of a reduced myofibroblast activity [51,52]. Such myofibroblasts are responsible for

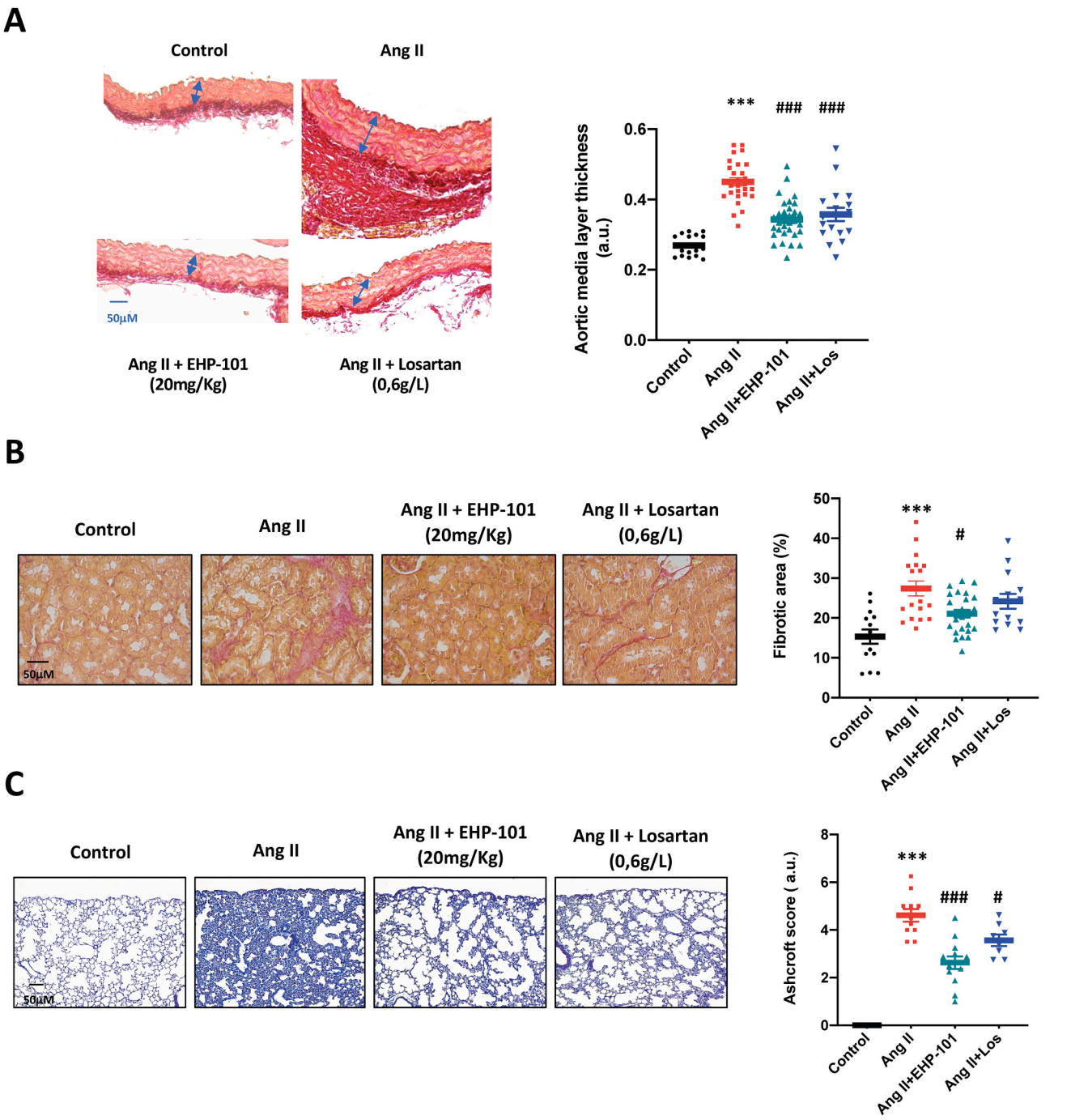

Fig. 8. EHP-101 treatment inhibits increased aortic media thickness, renal and lung fibrosis induced by Ang II. A. Representative images of aortic sections for Sirius red in preventive model (left panel) and the quantification of respective measurements on aorta sections (right panel). Blue arrows indicate aortic media. B. Representative photomicrographs of renal tissue from Ang II mouse therapeutic model stained with picrosirius red (left panel) and representative results for quantification of respective measurements of collagen area in kidney (right panel). C. Representative images of Masson's trichrome staining from lung (left panel) and their quantification by Ashcroft score (right). Data are expressed as median ± interquartile range with statistical comparison between Ang II–treated wild-type mice and all other conditions. For all these area measurements, three to four sections from a sample from six to eight mice per group were analyzed ***$p < 0.001$ *vs* control group; ###$p < 0.001$, #$p < 0.05$ *vs* Ang II group.

"executing" the TGF-β driven fibrosis. Of note is the similarity between the transcriptomic signatures observed in response to EHP-101 and Losartan, taking into account the different mechanism of action of both compounds. The main limitation of this study is that we do not have demonstrated the direct participation of E2F targets genes in the efficacy of EHP-101 on Ang-II-induced cardiac and other organs fibrosis and genetic experiments are needed to validate this novel mechanism of action.

Funding

This work was supported by the Ministerio de Economía y Competitividad (MINECO) (grant number SAF2017-87701-R (EM) and it is co-financed with the European Union FEDER funds. It was also partially supported by Emerald Health Pharmaceuticals (San Diego, USA).

CRediT authorship contribution statement

All the authors approved the final manuscript.

Declaration of Competing Interest

The authors declare the following financial interests/personal relationships which may be considered as potential competing interests: Carmen Navarrete and Adela García-Martín are employees of Emerald Health Pharmaceuticals. Eduardo Muñoz is Chief Scientific Officer of Emerald Health Pharmaceuticals. Giovanni Appendino is a member of the Scientific Advisory Board of Emerald Health Pharmaceuticals.

Ethics approval and consent to participate

All experiments with laboratory animals were conducted according to European guidelines (directive 2010/63/EU). Ethics Committee on Animal Experimentation at the University of Córdoba (Córdoba, Spain) approved all the procedures described in this study (protocol number: 23/03/2018/034).

Conflict of interest

Carmen Navarrete and Adela García-Martín are employees of Emerald Health Pharmaceuticals. Eduardo Muñoz is Chief Scientific Officer of Emerald Health Pharmaceuticals. Giovanni Appendino is a member of the Scientific Advisory Board of Emerald Health Pharmaceuticals.

Author contributions

AGM, CN and MEP conducted *in vivo* and *in vitro* experiments; MGR performed the bioinformatic analysis; DC and GA synthesized Ajulemic acid. AGM and EM managed, designed the overall study and wrote the manuscript. All the authors approved the final manuscript.

Appendix A. Supporting information

Supplementary data associated with this article can be found in the online version at doi:10.1016/j.biopha.2021.112007.

References

[1] L.A. Murtha, M.J. Schuliga, N.S. Mabotuwana, S.A. Hardy, D.W. Waters, J. K. Burgess, D.A. Knight, A.J. Boyle, The processes and mechanisms of cardiac and pulmonary fibrosis, Front Physiol. 8 (2017) 777, https://doi.org/10.3389/fphys.2017.00777.

[2] M. Writing Group, D. Mozaffarian, E.J. Benjamin, A.S. Go, D.K. Arnett, M.J. Blaha, M. Cushman, S.R. Das, S. de Ferranti, J.P. Despres, H.J. Fullerton, V.J. Howard, M. D. Huffman, C.R. Isasi, M.C. Jimenez, S.E. Judd, B.M. Kissela, J.H. Lichtman, L. D. Lisabeth, S. Liu, R.H. Mackey, D.J. Magid, D.K. McGuire, E.R. Mohler 3rd, C. S. Moy, P. Muntner, M.E. Mussolino, K. Nasir, R.W. Neumar, G. Nichol, L. Palaniappan, D.K. Pandey, M.J. Reeves, C.J. Rodriguez, W. Rosamond, P. D. Sorlie, J. Stein, A. Towfighi, T.N. Turan, S.S. Virani, D. Woo, R.W. Yeh, M. B. Turner, C. American Heart Association Statistics, S. Stroke Statistics, Heart Disease and Stroke Statistics-2016 update: a report from the American Heart Association, Circulation 133 (4) (2016) e38–e360, https://doi.org/10.1161/CIR.0000000000000350.

[3] C. Jellis, J. Martin, J. Narula, T.H. Marwick, Assessment of nonischemic myocardial fibrosis, J. Am. Coll. Cardiol. 56 (2) (2010) 89–97, https://doi.org/10.1016/j.jacc.2010.02.047.

[4] M. Disertori, M. Mase, F. Ravelli, Myocardial fibrosis predicts ventricular tachyarrhythmias, Trends Cardiovasc Med 27 (5) (2017) 363–372, https://doi.org/10.1016/j.tcm.2017.01.011.

[5] B.C. Berk, K. Fujiwara, S. Lehoux, ECM remodeling in hypertensive heart disease, J. Clin. Investig. 117 (3) (2007) 568–575, https://doi.org/10.1172/JCI31044.

[6] M.J. Ivey, M.D. Tallquist, Defining the cardiac fibroblast, Circ. J. 80 (11) (2016) 2269–2276, https://doi.org/10.1253/circj.CJ-16-1003.

[7] R.E. Schmieder, K.F. Hilgers, M.P. Schlaich, B.M. Schmidt, Renin-angiotensin system and cardiovascular risk, Lancet 369 (9568) (2007) 1208–1219, https://doi.org/10.1016/S0140-6736(07)60242-6.

[8] S.J. Forrester, G.W. Booz, C.D. Sigmund, T.M. Coffman, T. Kawai, V. Rizzo, R. Scalia, S. Eguchi, Angiotensin II signal transduction: an update on mechanisms of physiology and pathophysiology, Physiol. Rev. 98 (3) (2018) 1627–1738, https://doi.org/10.1152/physrev.00038.2017.

[9] U.M. Steckelings, T. Wollschlager, J. Peters, B.M. Henz, B. Hermes, M. Artuc, Human skin: source of and target organ for angiotensin II, Exp. Dermatol. 13 (3) (2004) 148–154, https://doi.org/10.1111/j.0906-6705.2004.0139.x.

[10] J. Wang, L. Chen, B. Chen, A. Meliton, S.Q. Liu, Y. Shi, T. Liu, D.K. Deb, J. Solway, Y.C. Li, Chronic activation of the renin-angiotensin system induces lung fibrosis, Sci. Rep. 5 (2015) 15561, https://doi.org/10.1038/srep15561.

[11] S.A. Mezzano, M. Ruiz-Ortega, J. Egido, Angiotensin II and renal fibrosis, Hypertension 38 (3 Pt 2) (2001) 635–638, https://doi.org/10.1161/hy09t1.094234.

[12] H.H. Sigusch, S.E. Campbell, K.T. Weber, Angiotensin II-induced myocardial fibrosis in rats: role of nitric oxide, prostaglandins and bradykinin, Cardiovasc Res 31 (4) (1996) 546–554.

[13] J. Sadoshima, Cytokine actions of angiotensin II, Circ. Res 86 (12) (2000) 1187–1189, https://doi.org/10.1161/01.res.86.12.1187.

[14] J.R. Gomolak, S.P. Didion, Angiotensin II-induced endothelial dysfunction is temporally linked with increases in interleukin-6 and vascular macrophage accumulation, Front Physiol. 5 (2014) 396, https://doi.org/10.3389/fphys.2014.00396.

[15] S. Kim, H. Iwao, Molecular and cellular mechanisms of angiotensin II-mediated cardiovascular and renal diseases, Pharm. Rev. 52 (1) (2000) 11–34.

[16] M.J. Sopel, N.L. Rosin, T.D. Lee, J.F. Legare, Myocardial fibrosis in response to Angiotensin II is preceded by the recruitment of mesenchymal progenitor cells, Lab. Investig. 91 (4) (2011) 565–578, https://doi.org/10.1038/labinvest.2010.190.

[17] A.R. Brasier, A. Recinos 3rd, M.S. Eledrisi, Vascular inflammation and the renin-angiotensin system, Arterioscler. Thromb. Vasc. Biol. 22 (8) (2002) 1257–1266, https://doi.org/10.1161/01.atv.0000021412.56621.a2.

[18] Q. Zhao, M. Ishibashi, K. Hiasa, C. Tan, A. Takeshita, K. Egashira, Essential role of vascular endothelial growth factor in angiotensin II-induced vascular inflammation and remodeling, Hypertension 44 (3) (2004) 264–270, https://doi.org/10.1161/01.HYP.0000138688.78906.6b.

[19] S.L. Lai, R. Marin-Juez, D.Y.R. Stainier, Immune responses in cardiac repair and regeneration: a comparative point of view, Cell Mol. Life Sci. 76 (7) (2019) 1365–1380, https://doi.org/10.1007/s00018-018-2995-5.

[20] N.G. Frangogiannis, C.W. Smith, M.L. Entman, The inflammatory response in myocardial infarction, Cardiovasc. Res. 53 (1) (2002) 31–47, https://doi.org/10.1016/s0008-6363(01)00434-5.

[21] F.C. Simoes, T.J. Cahill, A. Kenyon, D. Gavriouchkina, J.M. Vieira, X. Sun, D. Pezzolla, C. Ravaud, E. Masmanian, M. Weinberger, S. Mayes, M.E. Lemieux, D. N. Barnette, M. Gunadasa-Rohling, R.M. Williams, D.R. Greaves, L.A. Trinh, S. E. Fraser, S.L. Dallas, R.P. Choudhury, T. Sauka-Spengler, P.R. Riley, Macrophages directly contribute collagen to scar formation during zebrafish heart regeneration and mouse heart repair, Nat. Commun. 11 (1) (2020) 600, https://doi.org/10.1038/s41467-019-14263-2.

[22] E. Caglayan, B. Stauber, A.R. Collins, C.J. Lyon, F. Yin, J. Liu, S. Rosenkranz, E. Erdmann, L.E. Peterson, R.S. Ross, R.K. Tangirala, W.A. Hsueh, Differential roles of cardiomyocyte and macrophage peroxisome proliferator-activated receptor gamma in cardiac fibrosis, Diabetes 57 (9) (2008) 2470–2479, https://doi.org/10.2337/db07-0924.

[23] M. Asakawa, H. Takano, T. Nagai, H. Uozumi, H. Hasegawa, N. Kubota, T. Saito, Y. Masuda, T. Kadowaki, I. Komuro, Peroxisome proliferator-activated receptor gamma plays a critical role in inhibition of cardiac hypertrophy in vitro and in vivo, Circulation 105 (10) (2002) 1240–1246, https://doi.org/10.1161/hc1002.105225.

[24] S. Marquart, P. Zerr, A. Akhmetshina, K. Palumbo, N. Reich, M. Tomcik, A. Horn, C. Dees, M. Engel, J. Zwerina, O. Distler, G. Schett, J.H. Distler, Inactivation of the cannabinoid receptor CB1 prevents leukocyte infiltration and experimental fibrosis, Arthritis Rheum. 62 (11) (2010) 3467–3476, https://doi.org/10.1002/art.27642.

[25] C. del Río, C. Navarrete, J.A. Collado, M.L. Bellido, M. Gómez-Cañas, M.R. Pazos, J. Fernández-Ruiz, F. Pollastro, G. Appendino, M.A. Calzado, I. Cantarero, E. Muñoz, The cannabinoid quinol VCE-004.8 alleviates bleomycin-induced scleroderma and exerts potent antifibrotic effects through peroxisome proliferator-activated receptor-γ and CB2 pathways, Sci. Rep. 6 (2016) 21703, https://doi.org/10.1038/srep21703.

[26] A. Garcia-Martin, M. Garrido-Rodriguez, C. Navarrete, C. Del Rio, M.L. Bellido, G. Appendino, M.A. Calzado, E. Munoz, EHP-101, an oral formulation of the cannabidiol aminoquinone VCE-004.8, alleviates bleomycin-induced skin and lung fibrosis, Biochem. Pharmacol. 157 (2018) 304–313, https://doi.org/10.1016/j.bcp.2018.07.047.

[27] A. Garcia-Martin, M. Garrido-Rodriguez, C. Navarrete, D. Caprioglio, B. Palomares, J. DeMesa, A. Rollland, G. Appendino, E. Munoz, Cannabinoid derivatives acting as dual PPARgamma/CB2 agonists as therapeutic agents for systemic sclerosis, Biochem. Pharmacol. 163 (2019) 321–334, https://doi.org/10.1016/j.bcp.2019.02.029.

[28] M.A. Tepper, R.B. Zurier, S.H. Burstein, Ultrapure ajulemic acid has improved CB2 selectivity with reduced CB1 activity, Bioorg. Med. Chem. 22 (13) (2014) 3245–3251, https://doi.org/10.1016/j.bmc.2014.04.062.

[29] R. Sancho, A. Macho, L. de La Vega, M.A. Calzado, B.L. Fiebich, G. Appendino, E. Munoz, Immunosuppressive activity of endovanilloids: N-arachidonoyl-dopamine inhibits activation of the NF-kappa B, NFAT, and activator protein 1 signaling pathways, J. Immunol. 172 (4) (2004) 2341–2351, https://doi.org/10.4049/jimmunol.172.4.2341.

[30] T. Ashcroft, J.M. Simpson, V. Timbrell, Simple method of estimating severity of pulmonary fibrosis on a numerical scale, J. Clin. Pathol. 41 (4) (1988) 467–470.
[31] S. Chen, Y. Zhou, Y. Chen, J. Gu, fastp: an ultra-fast all-in-one FASTQ preprocessor, Bioinformatics 34 (17) (2018) i884–i890, https://doi.org/10.1093/bioinformatics/bty560.
[32] D. Kim, B. Langmead, S.L. Salzberg, HISAT: a fast spliced aligner with low memory requirements, Nat. Methods 12 (4) (2015) 357–360, https://doi.org/10.1038/nmeth.3317.
[33] Y. Liao, G.K. Smyth, W. Shi, featureCounts: an efficient general purpose program for assigning sequence reads to genomic features, Bioinformatics 30 (7) (2014) 923–930, https://doi.org/10.1093/bioinformatics/btt656.
[34] M.D. Robinson, D.J. McCarthy, G.K. Smyth, edgeR: a Bioconductor package for differential expression analysis of digital gene expression data, Bioinformatics 26 (1) (2010) 139–140, https://doi.org/10.1093/bioinformatics/btp616.
[35] A. Liberzon, C. Birger, H. Thorvaldsdottir, M. Ghandi, J.P. Mesirov, P. Tamayo, The Molecular Signatures Database (MSigDB) hallmark gene set collection, Cell Syst. 1 (6) (2015) 417–425, https://doi.org/10.1016/j.cels.2015.12.004.
[36] T. Wakatsuki, J. Schlessinger, E.L. Elson, The biochemical response of the heart to hypertension and exercise, Trends Biochem Sci. 29 (11) (2004) 609–617, https://doi.org/10.1016/j.tibs.2004.09.002.
[37] J. Liu, H. Li, S.H. Burstein, R.B. Zurier, J.D. Chen, Activation and binding of peroxisome proliferator-activated receptor gamma by synthetic cannabinoid ajulemic acid, Mol. Pharmacol. 63 (5) (2003) 983–992, https://doi.org/10.1124/mol.63.5.983.
[38] J.A. Wolfram, A. Liner, S.L. Richardson, X. Zhu, M.A. Smith, B.D. Hoit, H.G. Lee, The role of E2F1 in the development of hypertrophic cardiomyopathy, Int J. Clin. Exp. Pathol. 4 (5) (2011) 521–525.
[39] C. Navarrete, F. Carrillo-Salinas, B. Palomares, M. Mecha, C. Jimenez-Jimenez, L. Mestre, A. Feliu, M.L. Bellido, B.L. Fiebich, G. Appendino, M.A. Calzado, C. Guaza, E. Munoz, Hypoxia mimetic activity of VCE-004.8, a cannabidiol quinone derivative: implications for multiple sclerosis therapy, J. Neuroinflamm. 15 (1) (2018) 64, https://doi.org/10.1186/s12974-018-1103-y.
[40] L.O. Hanus, S.M. Meyer, E. Munoz, O. Taglialatela-Scafati, G. Appendino, Phytocannabinoids: a unified critical inventory, Nat. Prod. Rep. 33 (12) (2016) 1357–1392, https://doi.org/10.1039/c6np00074f.
[41] T. Matsusaka, I. Ichikawa, Biological functions of angiotensin and its receptors, Annu Rev. Physiol. 59 (1997) 395–412, https://doi.org/10.1146/annurev.physiol.59.1.395.
[42] T. Kawai, T. Masaki, S. Doi, T. Arakawa, Y. Yokoyama, T. Doi, N. Kohno, N. Yorioka, PPAR-gamma agonist attenuates renal interstitial fibrosis and inflammation through reduction of TGF-beta, Lab. Investig. 89 (1) (2009) 47–58, https://doi.org/10.1038/labinvest.2008.104.
[43] E. Wawryk-Gawda, K. Chlapek, M.K. Zarobkiewicz, M. Lis-Sochocka, P. Chylinska-Wrzos, A. Boguszewska-Czubara, M.A. Slawinski, A. Franczak, B. Jodlowska-Jedrych, G. Biala, CB2R agonist prevents nicotine induced lung fibrosis, Exp. Lung Res. 44 (7) (2018) 344–351, https://doi.org/10.1080/01902148.2018.1543368.
[44] G.L. Semenza, Regulation of mammalian O2 homeostasis by hypoxia-inducible factor 1, Annu Rev. Cell Dev. Biol. 15 (1999) 551–578, https://doi.org/10.1146/annurev.cellbio.15.1.551.
[45] Y. Zhang, X. Zhu, X. Huang, X. Wei, D. Zhao, L. Jiang, X. Zhao, Y. Du, Advances in understanding the effects of erythropoietin on renal fibrosis, Front. Med. 7 (2020) 47, https://doi.org/10.3389/fmed.2020.00047.
[46] J. Ikeda, T. Ichiki, H. Matsuura, E. Inoue, J. Kishimoto, A. Watanabe, C. Sankoda, S. Kitamoto, T. Tokunou, K. Takeda, G.H. Fong, K. Sunagawa, Deletion of phd2 in myeloid lineage attenuates hypertensive cardiovascular remodeling, J. Am. Heart Assoc. 2 (3) (2013), e000178, https://doi.org/10.1161/JAHA.113.000178.
[47] W. Bao, P. Qin, S. Needle, C.L. Erickson-Miller, K.J. Duffy, J.L. Ariazi, S. Zhao, A. R. Olzinski, D.J. Behm, G.C. Pipes, B.M. Jucker, E. Hu, J.J. Lepore, R.N. Willette, Chronic inhibition of hypoxia-inducible factor prolyl 4-hydroxylase improves ventricular performance, remodeling, and vascularity after myocardial infarction in the rat, J. Cardiovasc. Pharm. 56 (2) (2010) 147–155, https://doi.org/10.1097/FJC.0b013e3181e2bfef.
[48] Y. Jiang, C. Reynolds, C. Xiao, W. Feng, Z. Zhou, W. Rodriguez, S.C. Tyagi, J. W. Eaton, J.T. Saari, Y.J. Kang, Dietary copper supplementation reverses hypertrophic cardiomyopathy induced by chronic pressure overload in mice, J. Exp. Med 204 (3) (2007) 657–666, https://doi.org/10.1084/jem.20061943.
[49] M. Hinchcliff, Lenabasum for skin disease in patients with diffuse cutaneous systemic sclerosis, Arthritis Rheuma 72 (8) (2020) 1237–1240, https://doi.org/10.1002/art.41302.
[50] E.Y. Senchenkova, J. Russell, A. Yildirim, D.N. Granger, F.N.E. Gavins, Novel role of T cells and IL-6 (Interleukin-6) in angiotensin II-induced microvascular dysfunction, Hypertension 73 (4) (2019) 829–838, https://doi.org/10.1161/HYPERTENSIONAHA.118.12286.
[51] L. Song, L. Wang, F. Li, A. Yukht, M. Qin, H. Ruther, M. Yang, A. Chaux, P.K. Shah, B.G. Sharifi, Bone marrow-derived tenascin-C attenuates cardiac hypertrophy by controlling inflammation, J. Am. Coll. Cardiol. 70 (13) (2017) 1601–1615, https://doi.org/10.1016/j.jacc.2017.07.789.
[52] C.M. Tang, M. Zhang, L. Huang, Z.Q. Hu, J.N. Zhu, Z. Xiao, Z. Zhang, Q.X. Lin, X. L. Zheng, M. Yang, S.L. Wu, J.D. Cheng, Z.X. Shan, CircRNA_000203 enhances the expression of fibrosis-associated genes by derepressing targets of miR-26b-5p, Col1a2 and CTGF, in cardiac fibroblasts, Sci. Rep. 7 (2017) 40342, https://doi.org/10.1038/srep40342.
[53] N. Dyson, The regulation of E2F by pRB-family proteins, Genes Dev. 12 (15) (1998) 2245–2262, https://doi.org/10.1101/gad.12.15.2245.
[54] I.L. Flink, S. Oana, N. Maitra, J.J. Bahl, E. Morkin, Changes in E2F complexes containing retinoblastoma protein family members and increased cyclin-dependent kinase inhibitor activities during terminal differentiation of cardiomyocytes, J. Mol. Cell Cardiol. 30 (3) (1998) 563–578, https://doi.org/10.1006/jmcc.1997.0620.
[55] D. Vara, K.A. Bicknell, C.H. Coxon, G. Brooks, Inhibition of E2F abrogates the development of cardiac myocyte hypertrophy, J. Biol. Chem. 278 (24) (2003) 21388–21394, https://doi.org/10.1074/jbc.M212612200.